Supporting Information for

A facile solution processable self-rectifying and sub-1 V operating memristor via oxygen vacancy gradient within TiO_2 single layer

Min Ho Park[a,b], *Jun Hyung Jeong*[a,b], *Wonsik Kim*[c], *Soohyung Park*[c,d], *Byeong Min Lim*[a,b], *Hong-Sub Lee*[a,b] *and Seong Jun Kang*[*,a,b]

[a] Department of Advanced Materials Engineering for Information and Electronics, Kyung Hee University, Yongin, 17104, Republic of Korea

[b] Integrated Education Program for Frontier Materials (BK21 Four), Kyung Hee University, Yongin, 17104, Republic of Korea

[c] Advanced Analysis Center, Korea Institute of Science and Technology, 5 Hwarang-ro 14-gil, Seongbuk-gu, Seoul 02792, Republic of Korea

[d] Division of Nano & Information Technology, KIST School, University of Science and Technology (UST), Seoul 02792, Republic of Korea

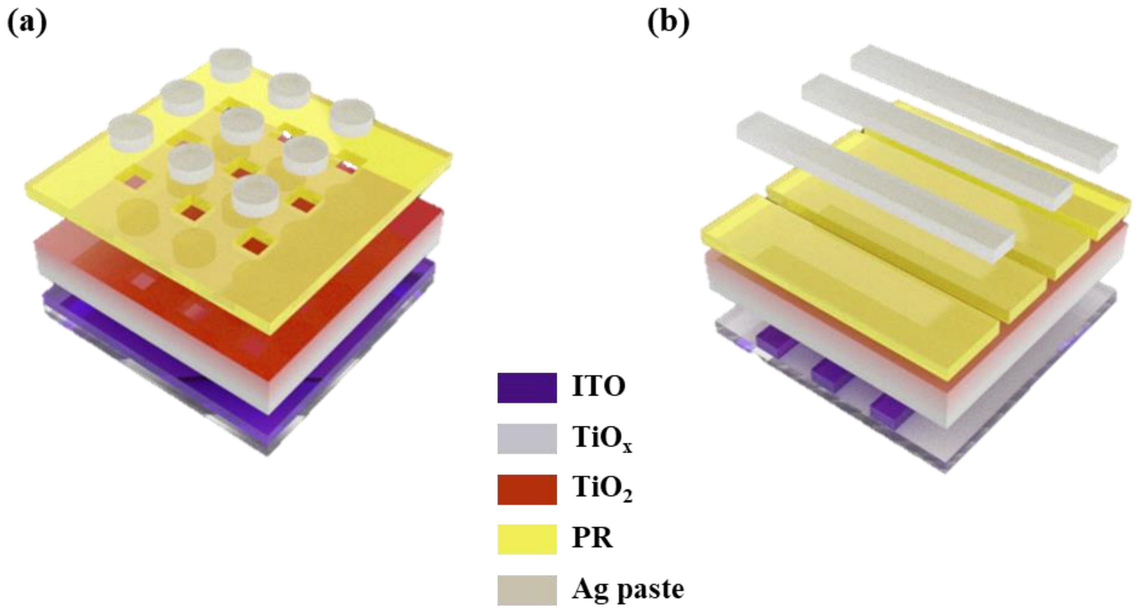

Fig. S1 Schematic structure of the a-TiO_2 based memristor. (a) Dot type device. (b) Crossbar type device.

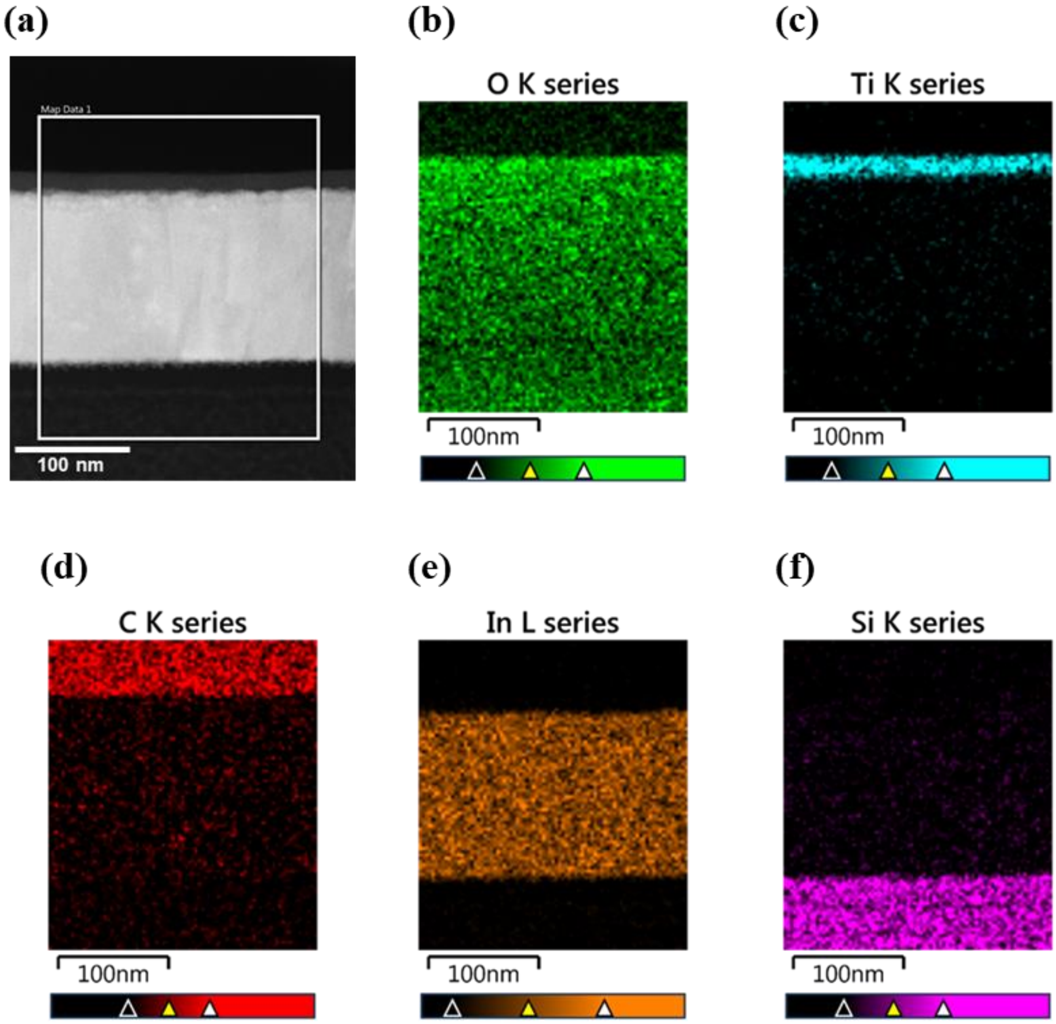

Fig. S2 (a) HR-TEM image of a-TiO_2 on the ITO substrate with 100 nm scale bar. (b-f) EDS mapping images of various elements (O, Ti, C, In, Si) in the a-TiO_2 film on the ITO substrate.

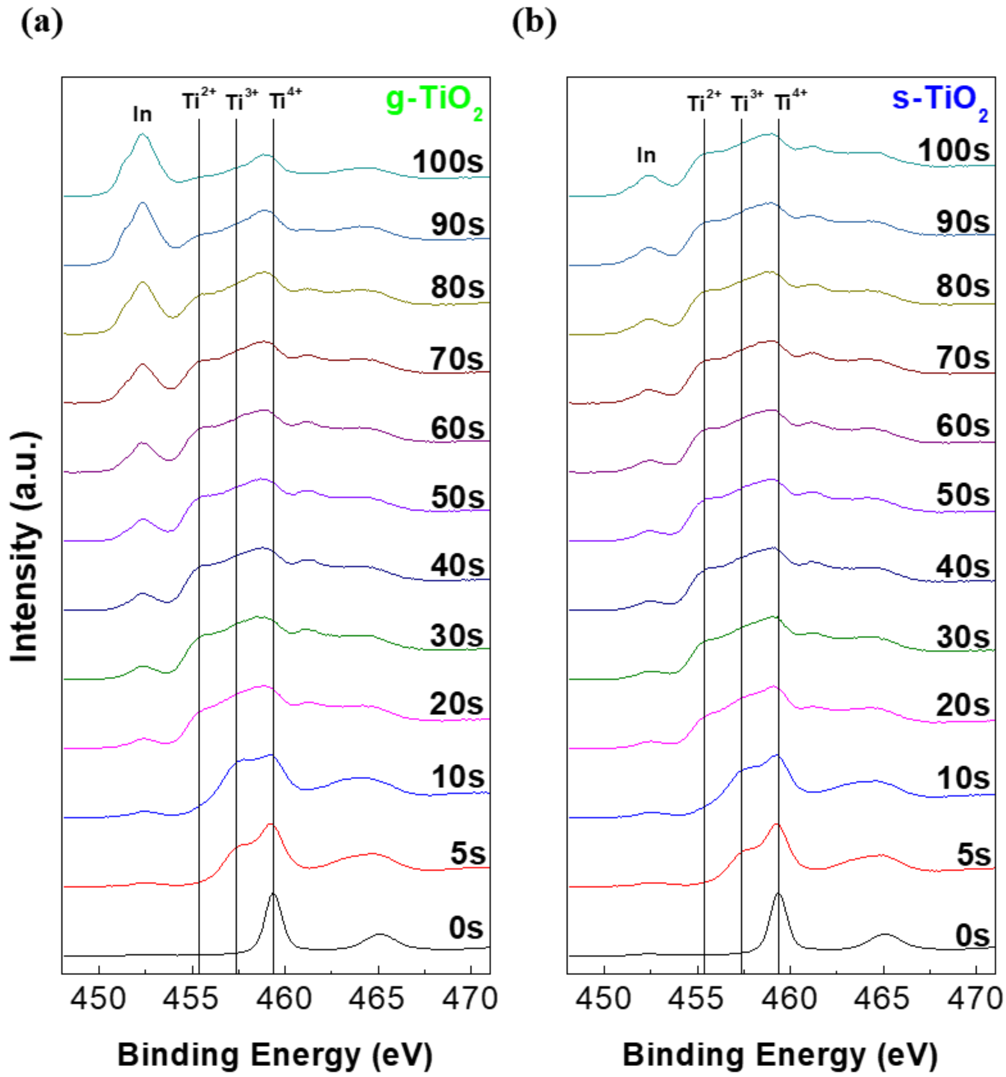

Fig. S3 XPS depth profile for Ti 2p (a) in g-TiO_2 film and (b) in s-TiO_2 film as the functions of Ar^+ sputtering time.

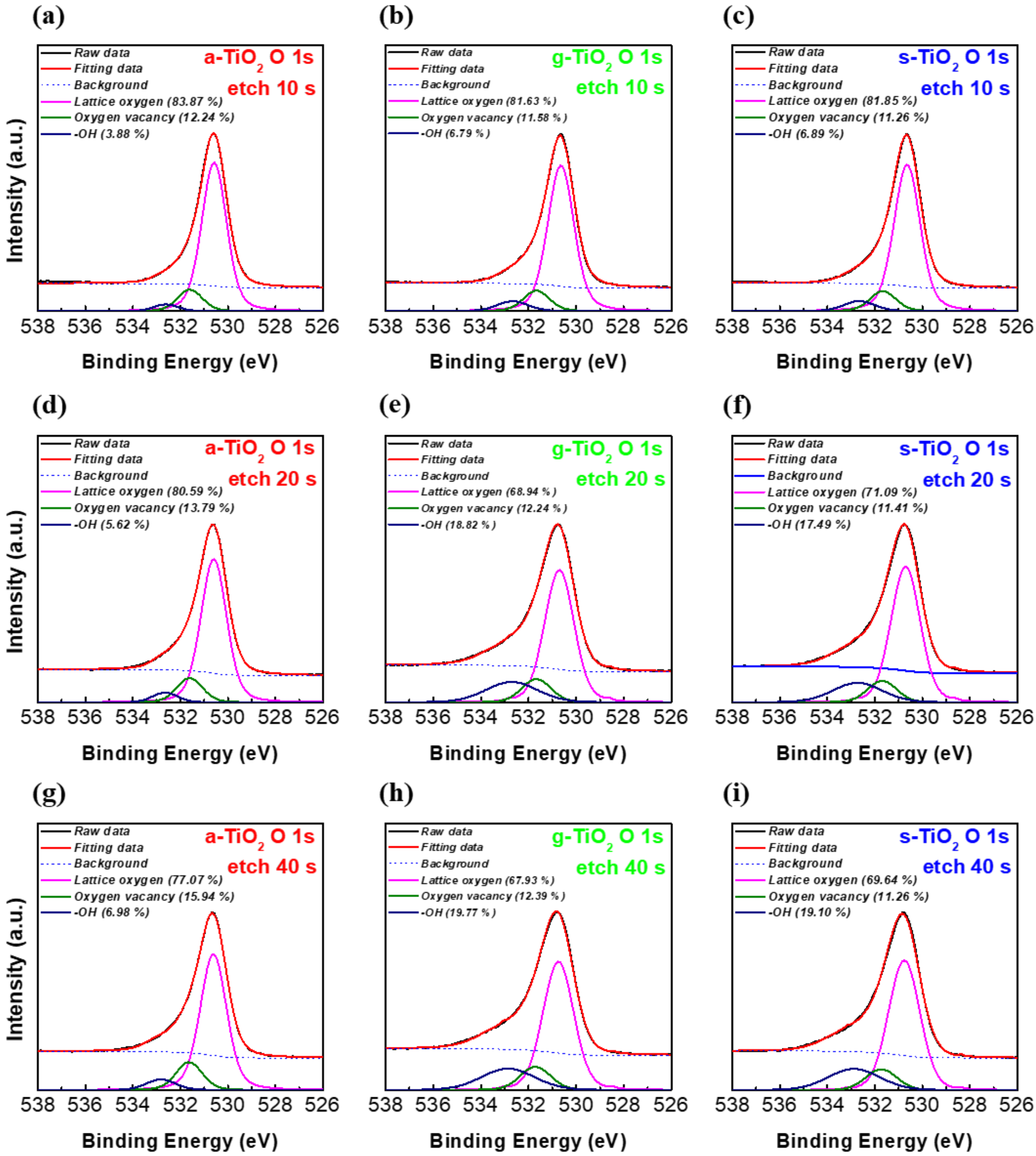

Fig. S4 XPS spectra of O 1s of (a,d,g) a-TiO_2,(b,e,h) g-TiO_2 and (c,f,i) s-TiO_2 films under different etching conditions.

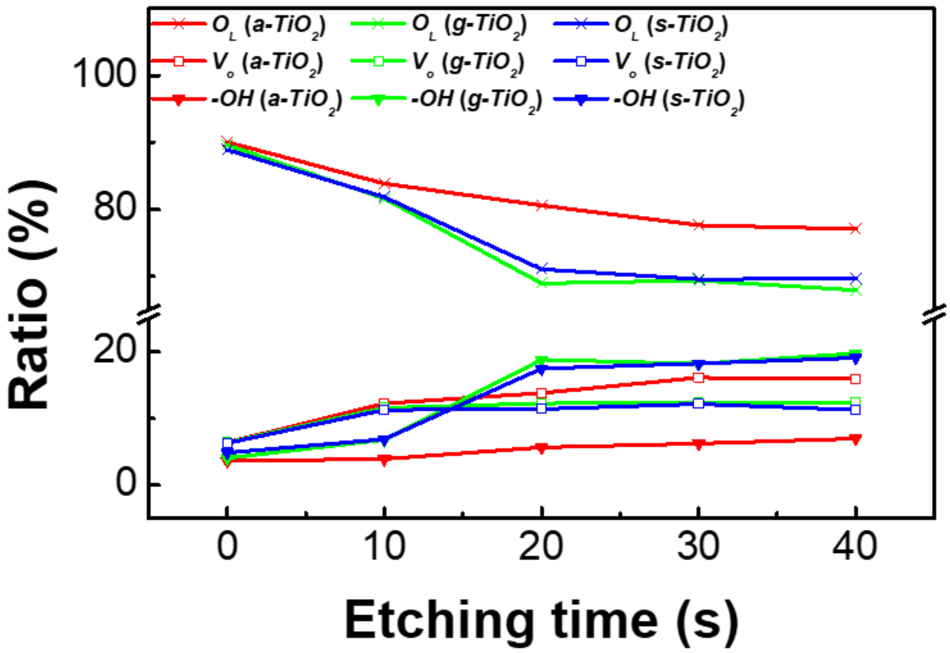

Fig. S5 Summarized ratio of deconvolution area of a-TiO_2, g-TiO_2 and s-TiO_2 films XPS O 1s spectra.

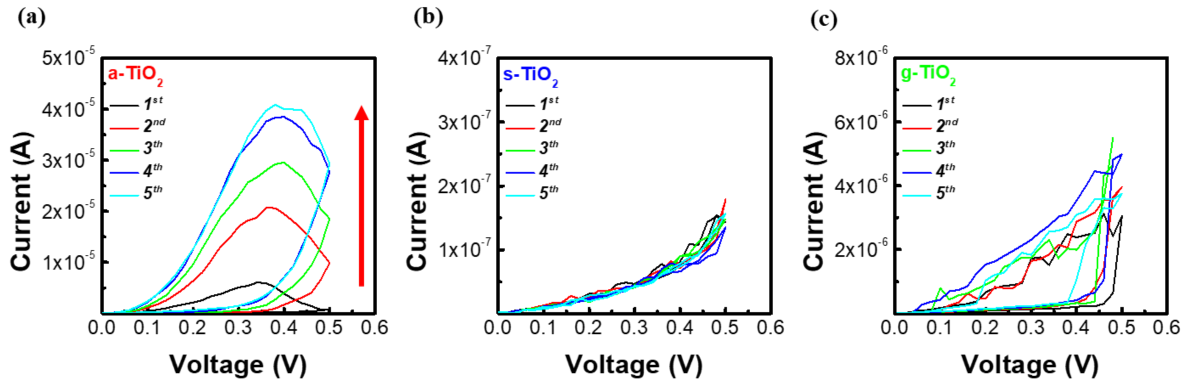

Fig. S6 *I-V* curves of memristors across 5 cycles, where positive voltage (0 V→0.5 V→0V) were applied.

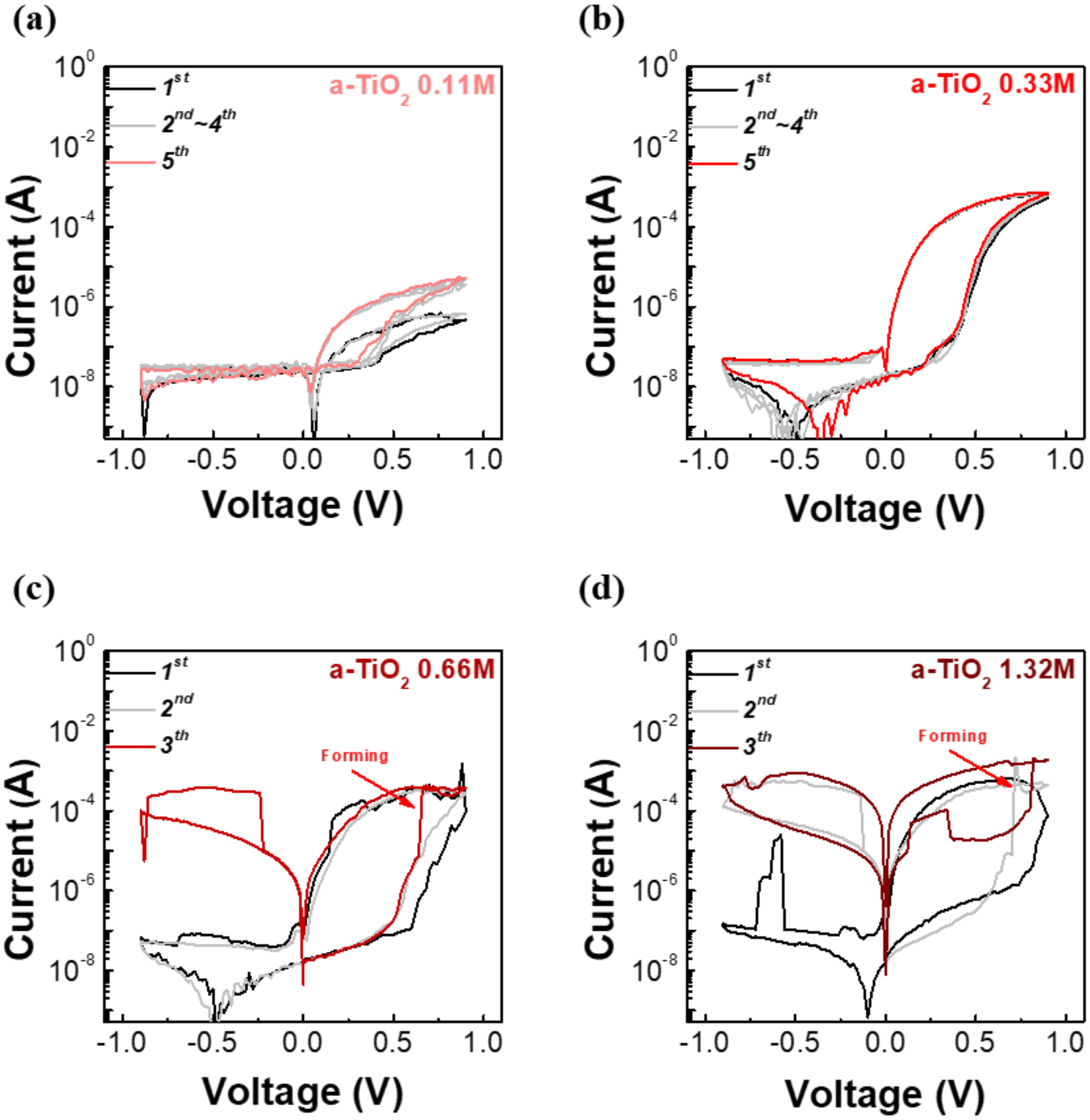

Fig. S7 *I-V* curves of a-TiO_2 based dot type memristors using various concentrations of solution.

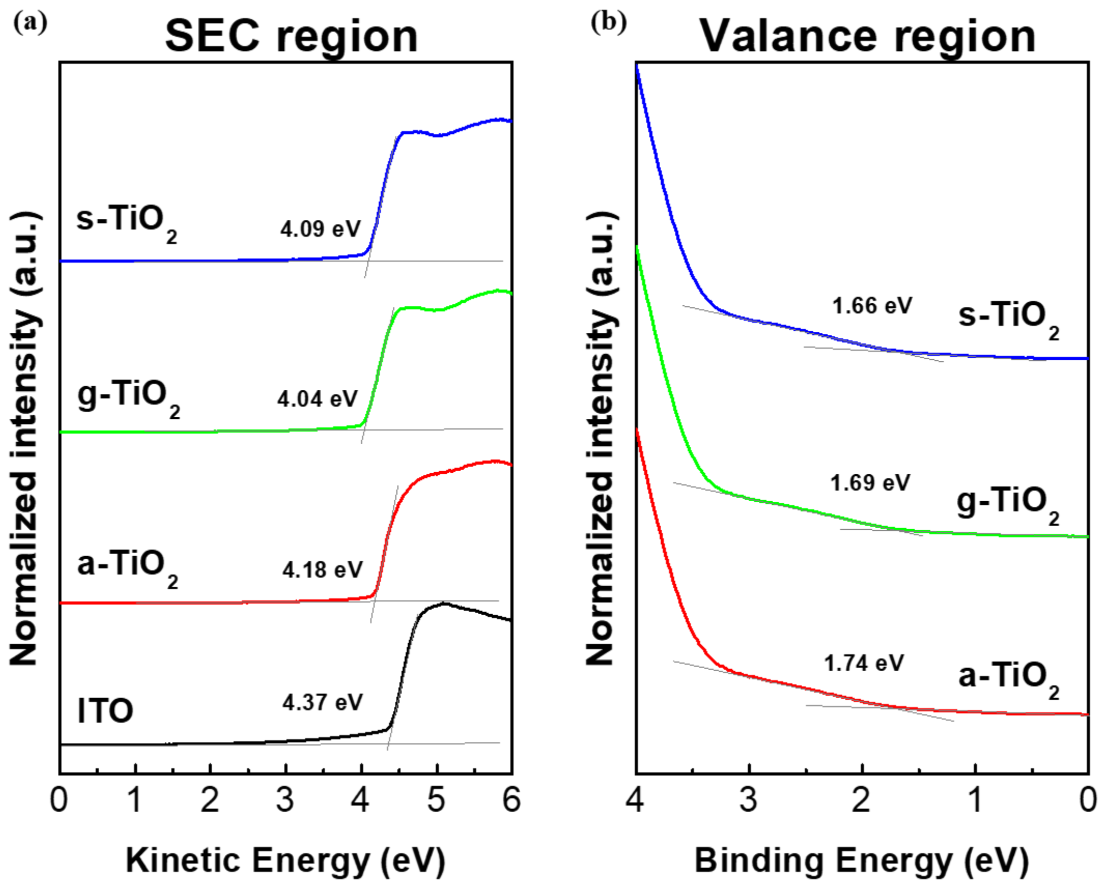

Fig. S8 UPS spectra of ITO, a-TiO_2, g-TiO_2 and s-TiO_2. (b) Secondary electron cut-off region. (c) Valance region.

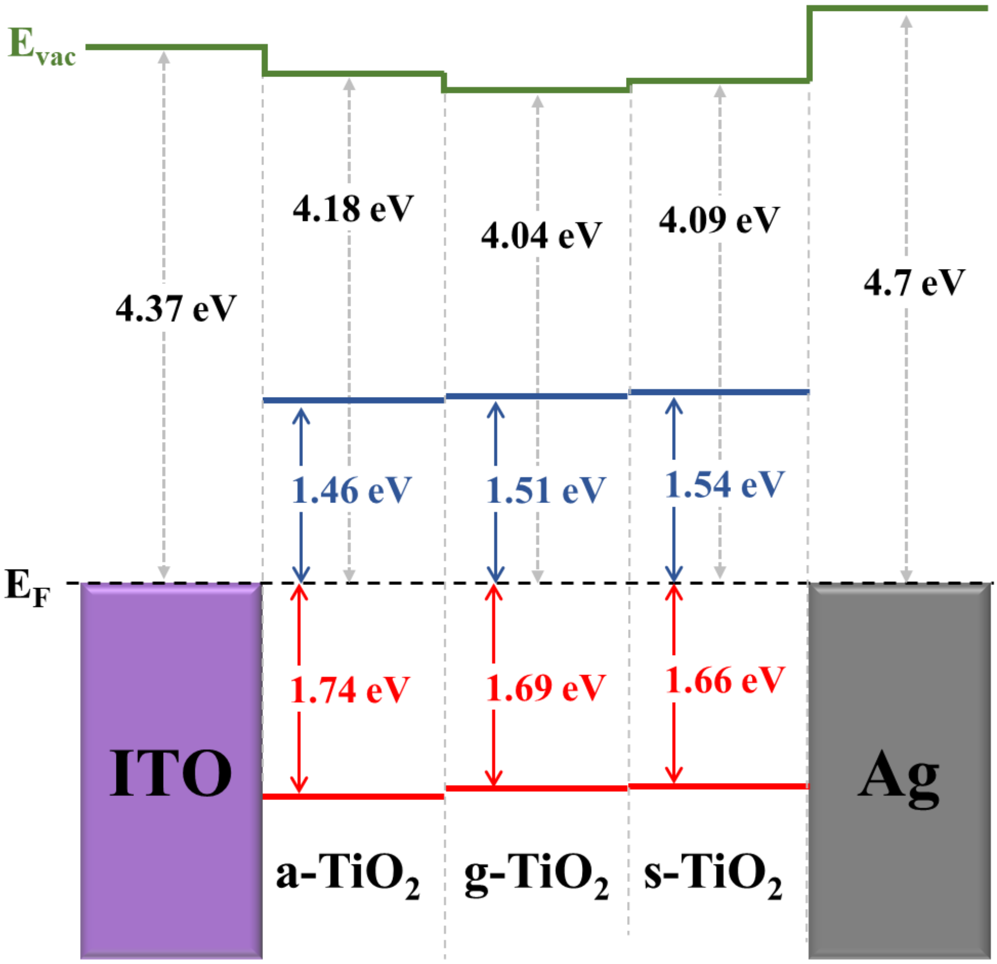

Fig. S9 Schematic energy band diagram of Ag/TiO_2/ITO memristors with aligned Fermi level.

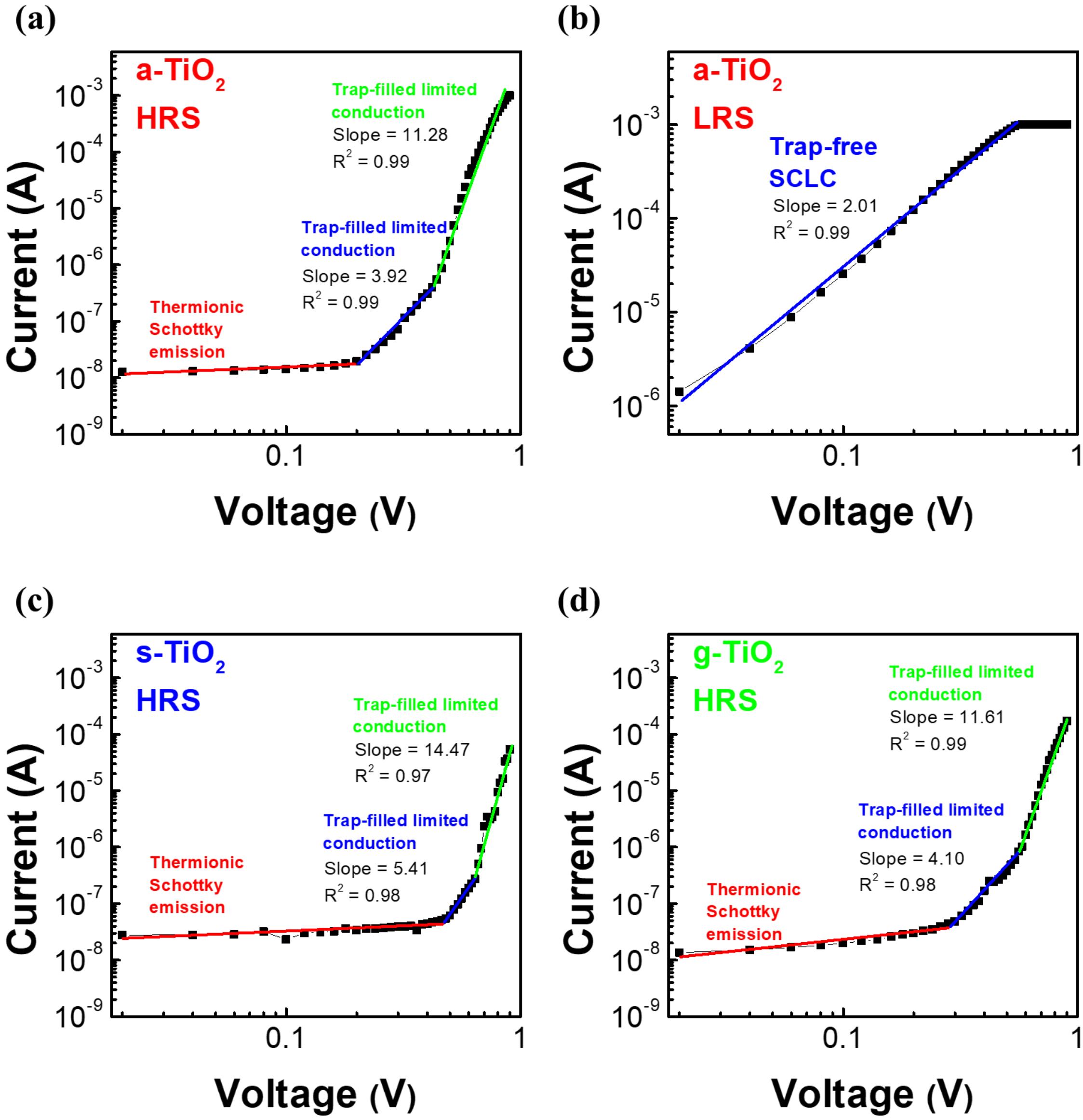

Fig. S10 log(I)-log(V) curves of the a-TiO_2, s-TiO_2 and g-TiO_2 to investigate the conduction mechanism.

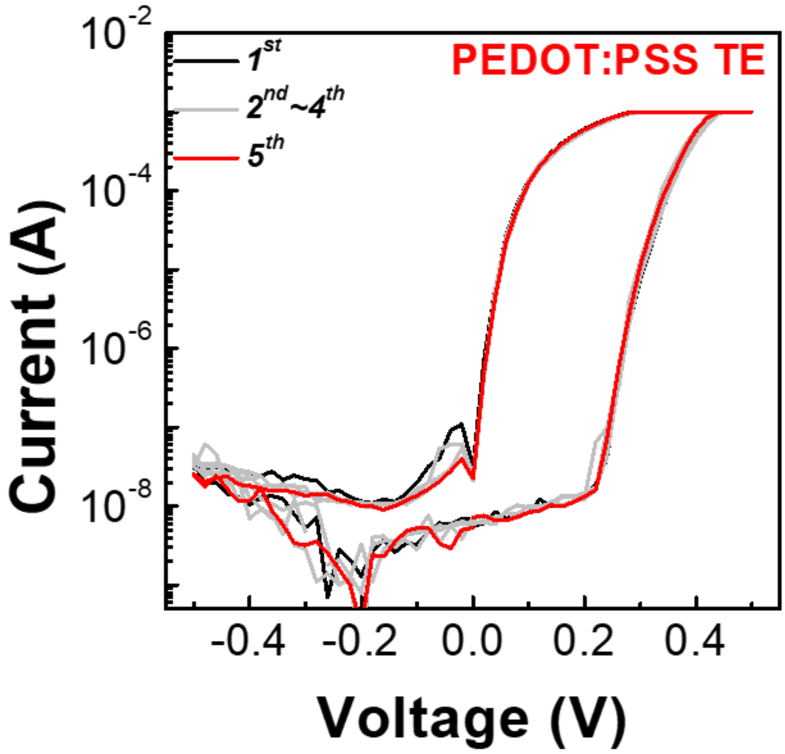

Fig. S11 *I-V* characteristics of a-TiO_2 based dot type memristor with PEDOT:PSS top electrode.

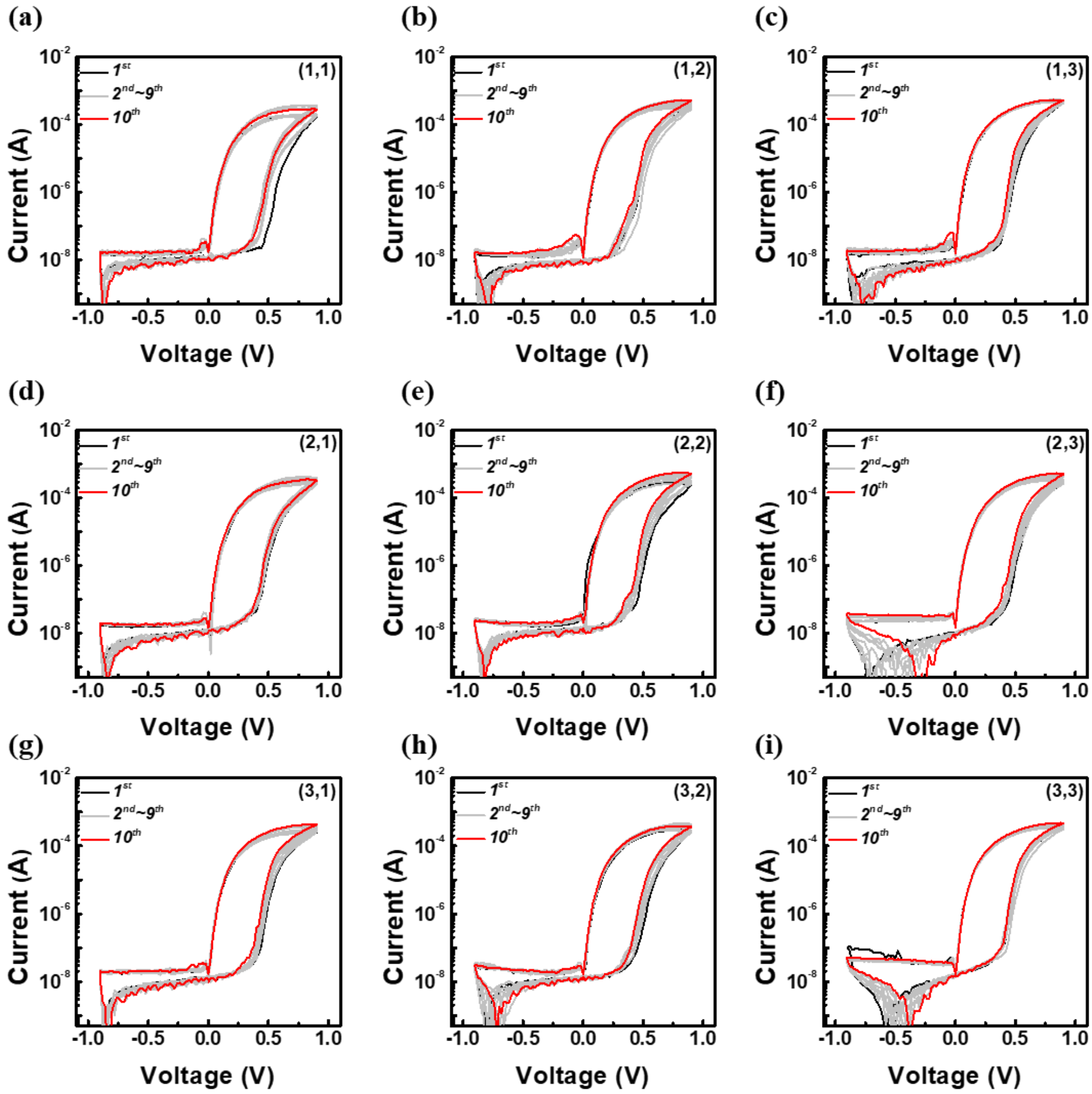

Fig. S12 *I-V* characteristics of a-TiO_2 based memristor in the 3 × 3 crossbar array.

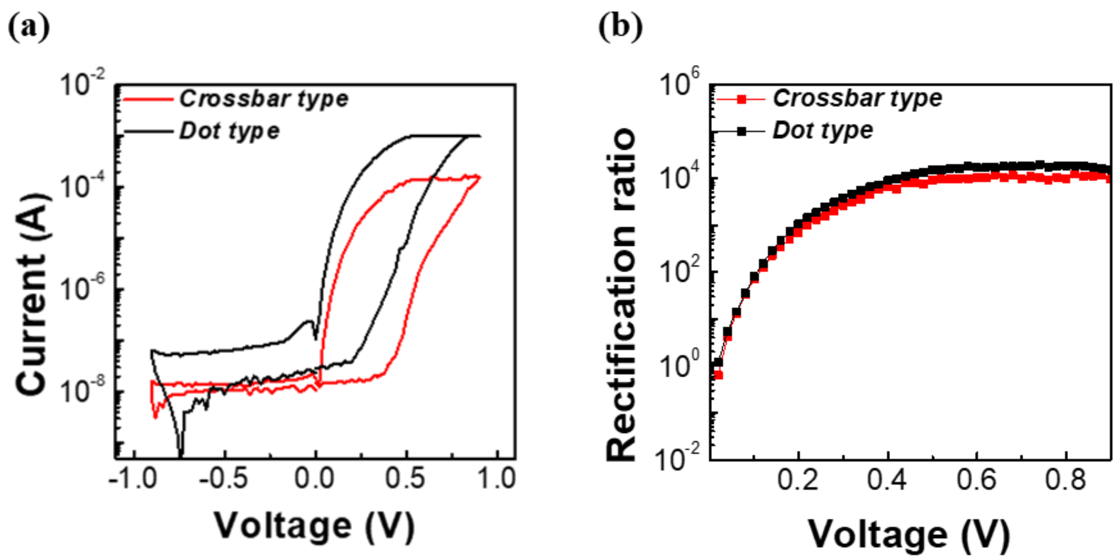

Fig. S13 (a) *I-V* curves, and (b) rectification ratio of dot type and crossbar type devices.

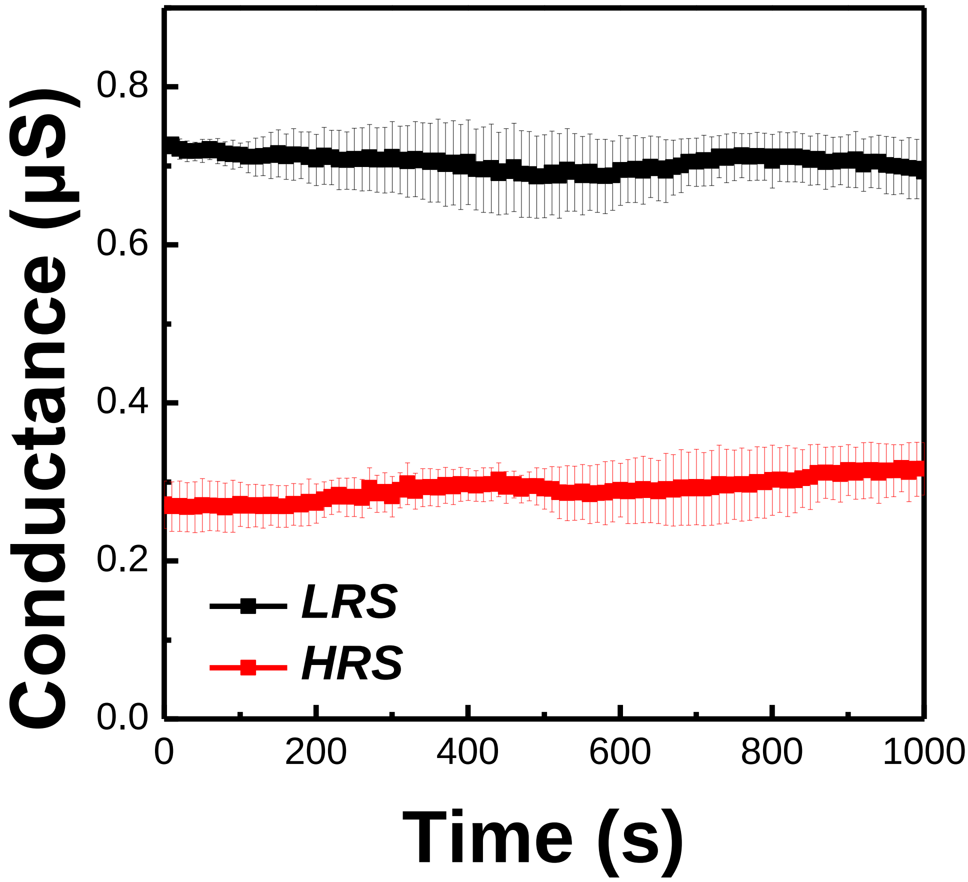

Fig. S14 The data retention of HRS and LRS recorded for an a-TiO_2 based memristor in the 3 × 3 crossbar array, with error bars.

	Structure	V_{set}	Rectification	Rectification ratio	On/off ratio	Size	Crossbar	Type	Ref
1	$Pt/Ti/HfO_x/TaO_x/TiN$	4 V	No		> 10	4~100 μm^2		Interface	67
2	$Pt/NbO_x/TiN$	1.5~2 V	No		> 10^2	0.16~16 μm^2		Filament	68
3	Ag/CTS-MoO_3/Mo	1~2 V	Restrictive	> 4×10^3	> 4×10^3	NA		Filament	69
4	$Pt/HfO_x/SiO_x/TiN$	3 V	No	NA	NA	NA		Filament	70
5	$Au/MAPb_3/Au$	2 V	No		> 10^8	2500 μm^2	8 × 8	Filament	71
6	$Au/HfSe_2/Ti$	0.74 V	No		> 10^2	25 μm^2	3 × 3	Filament	72
7	$Pt/TiO_x/HfO_2/Pt$	-5 V	Yes	> 10^3	NA	4 nm^2	3 × 3	Interface	73
8	$Au/TiO_2/Au$	3 V	Restrictive	NA	> 10^3	25~100 μm^2	32 × 32	Interface	74
9	$Ag/TiO_2/FTO$	5 V	No		> 10	12.55 mm^2		Interface	75
10	$Ag/TiO_2/FTO$	2 V	No		> 30	NA		Filament	76
This work	$Ag/TiO_2/TiO_x/ITO$	0.9 V	Yes	> 10^4	> 4×10^3	0.1~1 mm^2	3 × 3	Interface	

Table. S1 Comparative analysis of a-TiO_2 memristor performance relative to previous studies.